

Article

A Hydrodynamic–Elastic Numerical Case Study of a Solar Collector with a Double Enclosure Filled with Air and Fe₃O₄/Water Nanofluid

Rached Nciri ^{1,2}, Faris Alqurashi ³, Chaouki Ali ^{2,4} and Faouzi Nasri ^{3,*}

¹ Department of Mechanical Engineering, Higher Institute of Technological Studies of Gafsa, General Directorate of Technological Studies, Rades 2098, Tunisia; rachednciri@yahoo.fr

² Laboratory of Electro-Mechanical System, National Engineering School of Sfax-ENIS, B.P. W3038, University of Sfax, Sfax 3038, Tunisia; chaouki.ali.fsg@gmail.com

³ Mechanical Engineering Department, College of Engineering, University of Bisha, Bisha 61922, Saudi Arabia; fars421@hotmail.com

⁴ Department of Technological Paths, Faculty of Sciences of Gafsa, University of Gafsa, Gafsa 2112, Tunisia

* Correspondence: nasrifaouzi@yahoo.fr or fnasri@ub.edu.sa; Tel.: +966-59-032-0696

Abstract: This work deals with a numerical investigation of a hydrodynamic–elastic problem within the framework of a double enclosure solar collector technological configuration. The solar collector presents two enclosures separated by an elastic absorber wall. The upper enclosure is filled with air, whereas the lower one is filled with Fe₃O₄/water nanofluid. The mathematical model governing the thermal and flow behaviors of the considered nanofluid is elaborated. The effects of imposed hot temperatures, the Rayleigh number and air pressure on the nanofluid’s temperature contours, velocity magnitude distribution, temperature evolution, velocity magnitude evolution and Nusselt number evolutions are numerically investigated. The numerical results show and assess how the increase in the Rayleigh number affects convective heat transfer at the expense of the conductive one, as well as how much the Nusselt number and the nanofluid velocity magnitude and temperature are affected in a function of the imposed hot temperature type (uniformly or right-triangular distributed on the elastic absorber wall). Moreover, the results evaluate how increases in the air pressure applied on the elastic absorber wall affects the nanofluid’s temperature distribution.

Keywords: hydrodynamic; elastic wall; Fe₃O₄/water nanofluid; Rayleigh number; convection



Citation: Nciri, R.; Alqurashi, F.; Ali, C.; Nasri, F. A Hydrodynamic–Elastic Numerical Case Study of a Solar Collector with a Double Enclosure Filled with Air and Fe₃O₄/Water Nanofluid. *Processes* **2022**, *10*, 1195. <https://doi.org/10.3390/pr10061195>

Academic Editor: Rui A. Lima

Received: 19 April 2022

Accepted: 7 June 2022

Published: 15 June 2022

Publisher’s Note: MDPI stays neutral with regard to jurisdictional claims in published maps and institutional affiliations.



Copyright: © 2022 by the authors. Licensee MDPI, Basel, Switzerland. This article is an open access article distributed under the terms and conditions of the Creative Commons Attribution (CC BY) license (<https://creativecommons.org/licenses/by/4.0/>).

1. Introduction

Nanofluids can be simply seen as a base fluid (water, oil, ethylene glycol, etc.) in which nanosized particles (metals, oxides, carbon nanotubes, etc.) are in a colloidal suspension [1–4]. Since the thermal conductivity of the nanoparticles is higher than the base fluid, heat transfer is significantly enhanced compared to conventional base fluids. Thus, nanofluids can be potentially used in heat transfer technological applications [5–9], such as heat exchangers, chillers or engine cooling.

Computational Fluid Dynamics (CFD) is implemented in order to numerically investigate the thermal and flow performances of various nanofluids [10–15]. The considered nanofluids, characterized by certain physical properties, are filled in specific enclosures and are characterized by certain geometric and thermal properties. Heat sources and specific magnetic fields are taken into consideration. A MagnetoHydroDynamics (MHD) investigation is then introduced [16–19]. In CFD, nanofluids can be handled as either a single-phase or a two-phase fluid [20–22].

Several recent and relevant investigations dealing with MHD or Hydrodynamics (HD) coupled with elasticity are noted. Farooq A. et al. [23] investigated an MHD theoretical analysis for the heat transfer enhancement of three types of nanofluids. Accounting for the mass transpiration of a stretching wall (sheet), the results show that heat energy is

enhanced with thermal dissipation, heat sources and convective boundary conditions. Kamran A. et al. [24] carried out a numerical simulation of the heat transfer behavior of a two-dimensional Williamson nanofluid MHD flow over a permeable exponential stretching curved surface. A variable thermal conductivity and activation energy are considered. Hassan W. [25] carried out a numerical investigation of the MHD flow of engine oil using hybrid nanoparticles over a vertical stretching cylinder. The impacts of viscous dissipation and thermal radiation are considered. The results show that increases in the porosity variable reduce the fluid flow and enhance the temperature profile. Vishwanath B. Awati et al. [26] semi-numerically investigated in detail the steady-state convective boundary layer fluid flow of the heat and mass transfer behaviors of a nanofluid over a nonlinearly stretching sheet. The Haar wavelet collocation method is implemented. The results show that increases in the parameters associated with Brownian motion and thermophoresis induce a decrease in the local Nusselt number as well as an increase in the Sherwood number.

P. Hammachukiattikul et al. analytically investigated the impact of viscoplastic and thermal radiation on SA-based Cu-Fe₃O₄ hybrid nanofluid flow with a shrinking/stretching surface. The results show that the radiation heat source, the magnetic field as well as the Casson parameters enhance the thermal boundary layer thickness [27]. N.F.H. Mohd Sohut et al. [28] numerically investigated unsteady 3D flow over a stretching sheet in a rotating hybrid nanofluid. The results show that increases in nanoparticle volume fraction enhance the skin friction coefficient. The heat transfer rate at the surface and the skin friction coefficient are reduced when the rotating parameter increases. The results also show that thermal radiation and the unsteadiness parameter stimulate the temperature. Nor A. Yacoub [29] numerically investigated 3D rotating flow in water and kerosene-based nanofluids with single and multi-walled CNT nanoparticles over a shrinking/stretching surface. The results show that heat transfer is enhanced when the nanoparticle volume fraction or suction parameter increases, whereas it is reduced with increments in the rotating flow parameter. The results also show that kerosene-based nanofluids with multi-walled CNT nanoparticles permit better heat transfer rates. Ramzan M. et al. [30] numerically investigated a partially ionized 3D Casson nanoliquid flow over a porous stretched two-directional surface with C-C heat flux. A surface-catalyzed reaction is used in order to speed up the chemical reaction. The results show that the velocity profile is reduced as the Casson and porosity parameters increase, whereas it is enhanced when the Hall current increases.

Muhammad Mubashir Bhatti et al. [31] implemented a new computational technique called the successive local linearization method, denoted by SLLM. The goal is to numerically investigate the effect of activation energy on a magnetized nanofluid containing moveable gyrotactic microorganisms through a stretching elastic porous plate. The results show that the SLLM is both stable and flexible with respect to resolving transport problems processed by nonlinear magnetic materials. Furthermore, the proposed SLLM has shown its accuracy, efficiency and smoothness.

Shady M. Henein and Ahmed A. Abdel-Rehim [32] experimentally investigated the effects of using different weight ratios of a MgO/MWCNT-Water hybrid nanofluid on the thermal performance of an evacuated tube solar collector. The experiments were carried out at a 0.02% particle concentration and at different volume flow rates, varying from 1 to 3 L/min. The principal results show that the energy and the exergy efficiencies of the solar collector are enhanced with increases in the MWCNT weight ratio and the volume flow rate. The enhancement of the higher energy and exergy efficiencies reached, respectively, 55.83% and 77.14% for a MgO/MWCNT weight ratio in the order of (50:50). The better efficiency of the evacuated tube solar collector was performed for an MgO/MWCNT weight ratio of (50:50) for all the investigated volume flow rates.

Palash Soni et al. [33] carried out a Computational Fluid Dynamics numerical investigation (using Solid-Works flow simulation) about the effects of the helical tube pitch and coil diameter in the performance of a shell and helical tube heat exchanger (SHTHE) applying CuO/water and Al₂O₃/water nanofluids. The main results show that increases in the pitch and coil diameter enhance the effectiveness of the SHTHE. The higher effectiveness reaches

values of 0.5022 and 0.4928 for CuO/water and Al₂O₃/water nanofluid, respectively, at the pitch in the order of 0.018 m and the coil diameter in the order of 0.116 m.

Muhammad Imran et al. [34] numerically investigated the heat transfer and MHD effects associated with a hybrid SiC and TiO₂/kerosene oil nanofluid two-dimensional unsteady flow carried out over a flat horizontal porous surface with entropy generation. The effects of suction/injection velocity and the velocity ratio parameter on the fluid velocity profiles, as well as the effects of the nanoparticle volume fraction, Eckert number, velocity ratio parameter and shape factors on the thermal field, were investigated. Moreover, the effects of the Brinkman number and the Reynolds number on entropy generation was studied. Particular interest was paid towards the handling and solving of the partial differential equations that govern the considered problem. The principal results show that the thermal profile is enhanced with increases in the Eckert number and the nanoparticle volume fraction. Moreover, entropy generation is augmented with increases in the Brinkman number and Reynolds number.

Chetpelly Akshay [35] numerically investigated the thermal modeling of single and double-slope passive solar stills (SSSS and DSSS) in six Indian cities, representing different climatic zones. The thermal and yield performances were assessed. Hourly variations of the glass cover and basin water temperatures, as well as the heat transfer coefficients, were assessed. The main results show that the yield of DSSS over SSSS reached 63.37%, 57.91%, 55.59%, 44.30%, 6.15% and 34.29% on a winter day and 91.3%, 89.3%, 70.92%, 93.25%, 56.88% and 75.87% for the six cities.

The aim of this work is to numerically investigate a hydrodynamic–elastic problem within the framework of a double-enclosure solar collector technological configuration. The effects of the imposed hot temperature, Rayleigh number and air pressure on the thermal and flow performances were investigated for Fe₃O₄/water nanofluid.

The originality of our research work is that our proposed hydrodynamic–elastic numerical investigation is perfectly adapted to a specific technological configuration (with respect to dimension ratios of the enclosures, elastic wall absorber, type of the used nanofluid, type and location of the imposed cold and hot temperature, location of insulations, etc.) of a real solar air collector that we are working on in order to understand in depth and to considerably improve the control of its heat-transfer behavior. This is exactly our specific gap of knowledge to fill. Thus, the results of this investigation are very useful for us in the sense that it permits us to further develop solar air collectors with much more control on their thermal performance.

Section 2 states the considered hydrodynamic–elastic wall nanofluid problem. The governing mathematical modeling is carried out in Section 3. Section 4 details the solution methodology and convergence. Section 5 presents and discusses the numerical results. The conclusions are presented in Section 6.

2. Problem Statement

A hydrodynamic–elastic wall problem was numerically investigated within the framework of a solar collector technological configuration. The investigated solar collector (Figure 1) is composed of two enclosures separated by an elastic absorber wall. The upper enclosure is filled with air, whereas the lower one is filled with Fe₃O₄/water nanofluid. The hot air applies a certain pressure, inducing the stretching of the absorber plate. A hot temperature distribution is imposed on the absorber plate, whereas the cold temperature is imposed on the left and right walls, as depicted by Figure 1. The remaining walls are adiabatic. The thermophysical properties of the considered nanofluid are summarized in Table 1 [36–38]. The hot temperature distribution applied on the absorber plate influences both the nanofluid temperature contours and the nanofluid velocity magnitudes. The air pressure influences the nanofluid temperature contours.

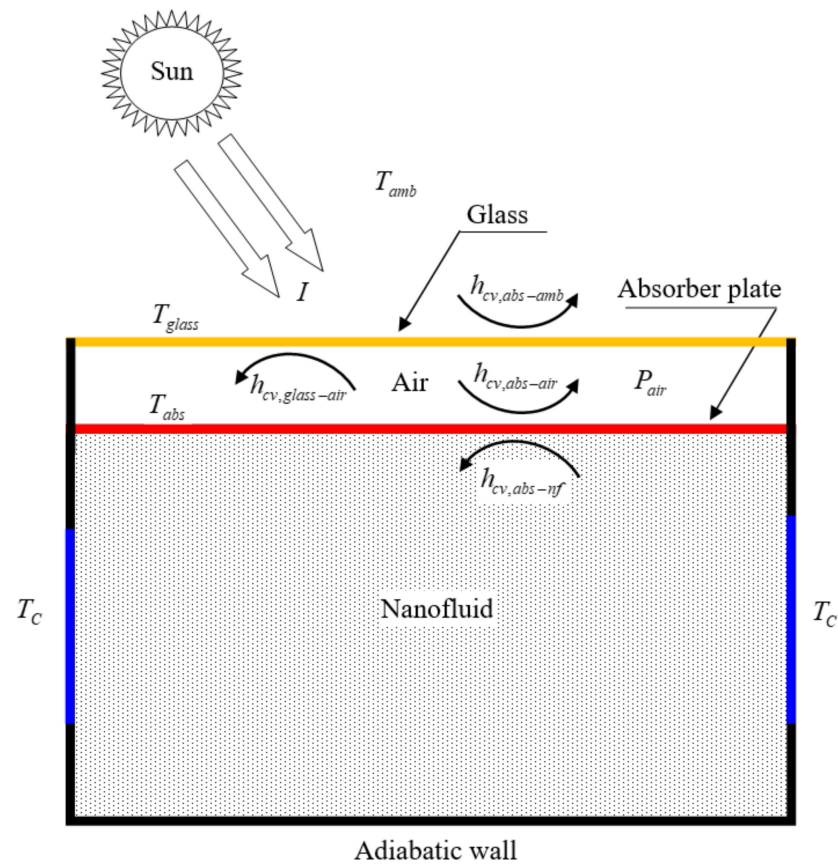


Figure 1. Investigated solar collector.

Table 1. Nanofluid thermophysical properties.

Nanofluid Characteristics	Fe ₃ O ₄ (Nanoparticles)	Water (Base Fluid)
Density ρ (kg/m ³)	5180	997.1
Specific heat capacity C_p (J/kgK)	670	4179
Thermal conductivity k (W/mK)	9.7	0.613

3. Mathematical Modeling

The mathematical model of the considered problem was formulated based on the following assumptions:

- Apart from the density, the thermophysical properties of the fluid are assumed to be constant.
- Density variations of the fluid are governed by the Boussinesq approximation in the buoyancy term.
- The wall separating air from the nanofluid is assumed to be elastic with Young's modulus E , Poisson's coefficient ν and density ρ_e .
- The nanofluid flow is assumed to be 2D, steady and laminar.
- Density variations of the nanofluid are governed by the Boussinesq approximation in the buoyancy term.

The nanofluid's motion with the elastic wall in the fluid–structure interaction model is governed by the arbitrary Lagrangian–Eulerian method. Navier–Stokes and energy conservation equations with effective thermophysical properties govern the flow and the thermal behavior of the nanofluid [39–42].

The mass conservation equation for the nanofluid domain is written as:

$$\nabla \cdot \vec{u} = 0 \quad (1)$$

The momentum conservation equation for the nanofluid domain is written as:

$$\rho_{nf}(\vec{u} - \vec{u}_g)\nabla \cdot \vec{u} = \nabla \cdot \overline{\overline{\sigma}}_{nf} + \rho_{nf}f_{b,nf}^{\rightarrow} \quad (2)$$

The energy conservation equation for the nanofluid domain is written as:

$$\vec{u}\nabla T = \alpha_{nf}\nabla^2 T \quad (3)$$

The equation for the solid domain of the fluid–structure interaction model is written as:

$$\rho_s \vec{a}_s = \nabla \cdot \overline{\overline{\sigma}}_s + \vec{f}_{b,s} \quad (4)$$

The nanofluid's effective density is written as:

$$\rho_{nf} = (1 - \phi)\rho_f + \phi\rho_p \quad (5)$$

The nanofluid's effective specific heat is written as:

$$(\rho C_p)_{nf} = (1 - \phi)(\rho C_p)_f + \phi(\rho C_p)_p \quad (6)$$

The nanofluid's effective coefficient of thermal expansion is written as:

$$(\rho\beta)_{nf} = (1 - \phi)(\rho\beta)_f + \phi(\rho\beta)_p \quad (7)$$

The nanofluid's effective thermal conductivity is written as:

$$k_{nf} = k_{st} + k_{Brownian} \quad (8)$$

where

$$k_{st} = k_f \frac{(k_p + 2k_f) - 2\phi(k_f - k_p)}{(k_p + 2k_f) + \phi(k_f - k_p)} \quad (9)$$

The nanofluid's effective viscosity is written as:

$$\mu_{nf} = \mu_f \frac{1}{1 - 34.87\left(\frac{D_p}{D_f}\right)^{-0.3} \phi^{1.03}} \quad (10)$$

The thermal boundary conditions are expressed as the following:

At the hot wall:

$$T = T_h \quad (11)$$

at the cold walls:

$$T = T_c \quad (12)$$

at the adiabatic wall:

$$\left. \frac{\partial T}{\partial n} \right| = 0 \quad (13)$$

The motion boundary conditions for the rigid walls are expressed as:

$$u = v = 0 \quad (14)$$

At the nanofluid–elastic structure interface:

- The displacement compatibility equation:

$$\vec{d}_f = \vec{d}_s \quad (15)$$

- The traction equilibrium equation:

$$\overline{\overline{\sigma_f}} = \overline{\overline{\sigma_s}} \quad (16)$$

4. Solution Methodology and Convergence

The solution methodology of the considered mathematical problem, globally, consists of three main steps:

- First step: The non-linear convective term (product of velocity and its derivative) is linearized using Newton linearization. An iterative scheme is implemented to calculate the obtained linearized term. Reasonable starting values of velocity and temperature, as well as an appropriate convergence criterion, are used.
- Second step: The first iteration of the obtained linearized hydrodynamic–elastic problem is solved using the Finite Element Method. The solution of the Stokes flow (Navier–Stokes neglecting the convective term) is used for the initial velocity and temperature values in order to obtain the first iteration of the considered hydrodynamic–elastic problem. It is worth noting that a stable solution for the Stokes flow is obtained if the velocity and temperature are interpolated with a higher order than the pressure.
- Third step: The considered hydrodynamic–elastic problem is iterated by assigning the last iteration velocity and temperature fields to the new iteration until reaching a converged solution.

The Finite Element Method is numerically implemented to solve the system of partial differential equations that constitute the mathematical model governing the considered hydrodynamic–elastic problem. As depicted by Figure 2, the investigated nanofluid and elastic absorber plate domains are subdivided into triangular elements: 11,262 domain elements and 964 boundary elements (Figure 2). The relative tolerance is set to a small enough value, ensuring the solution convergence stated by:

$$\left| \frac{\text{Current solution} - \text{Previous solution}}{\text{Current solution}} \right| < \varepsilon \quad (17)$$

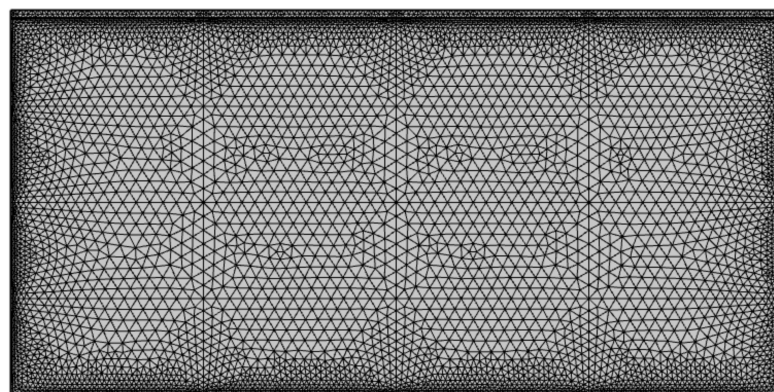


Figure 2. Meshing of the nanofluid and the elastic absorber plate.

5. Results and Discussion

5.1. Results Validation

Our computer code, as well as our solution methodology and convergence, are validated by implementing the same problem studied by Fatih Selimefendigil and Hakan F. Öztöp in their work [36]. The agreement is very good between our numerical results (depicted by Figure 3) and those carried out in [36] (Page 512; Figure 3. (c) Streamlines for $Ra_E = 5 \times 10^5$ and Figure 3. (e) Isotherms for $Ra_E = 10^4$). The considered results presented in [36] are not reprinted in the current article for reasons of possible copyright issues.

5.2. Combined Effect of Hot Temperature Distribution and Rayleigh Number

The combined effects of hot temperature distributions and the Rayleigh number on a nanofluid's temperature contours (Figure 4), velocity magnitude distribution (Figure 5), velocity magnitude evolution (Figure 6) and Nusselt number evolution (Figure 7) were numerically investigated.

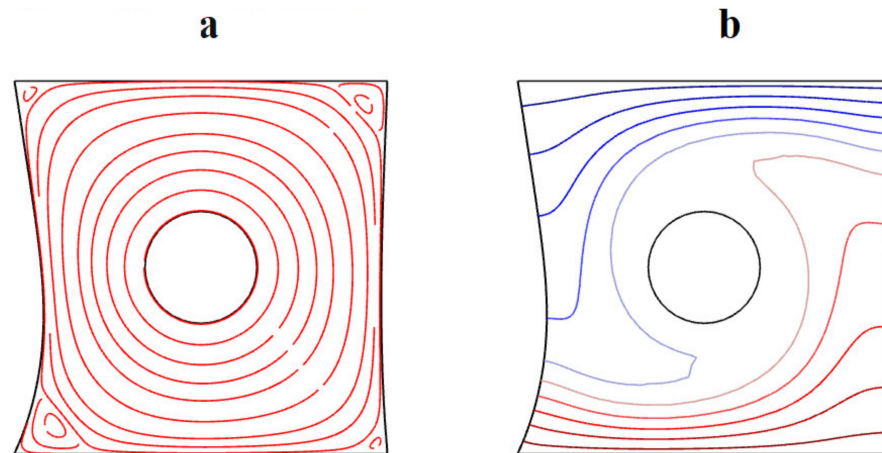


Figure 3. Streamlines (a) and Isotherms (b) for the validation of the current work results based on the results presented in [36] (page 512; Figure 3).

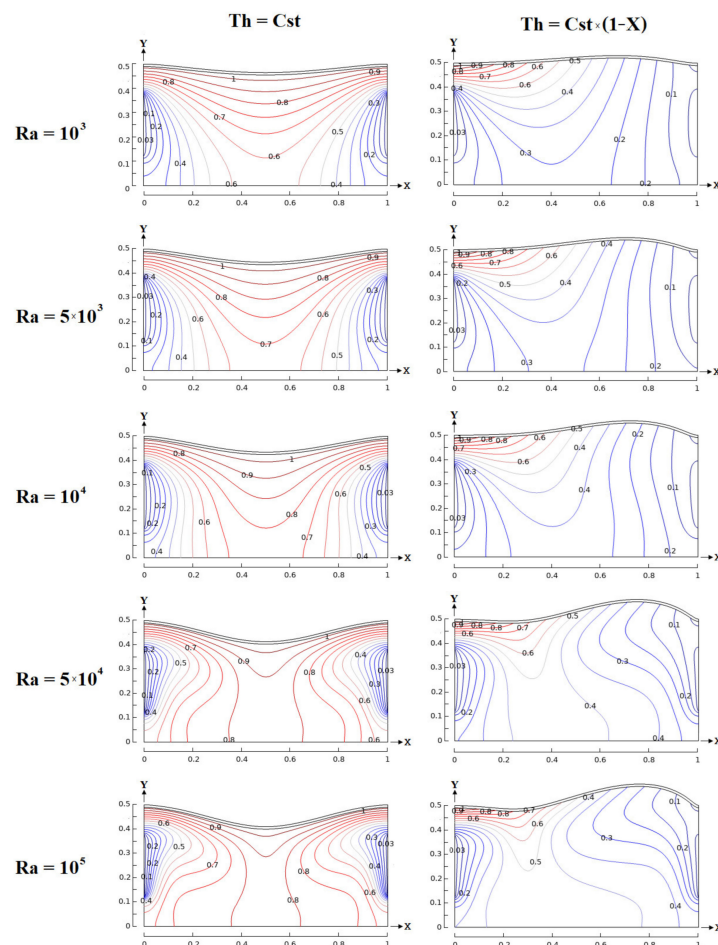


Figure 4. Combined effects of hot temperature distribution and Rayleigh number on nanofluid temperature contours.

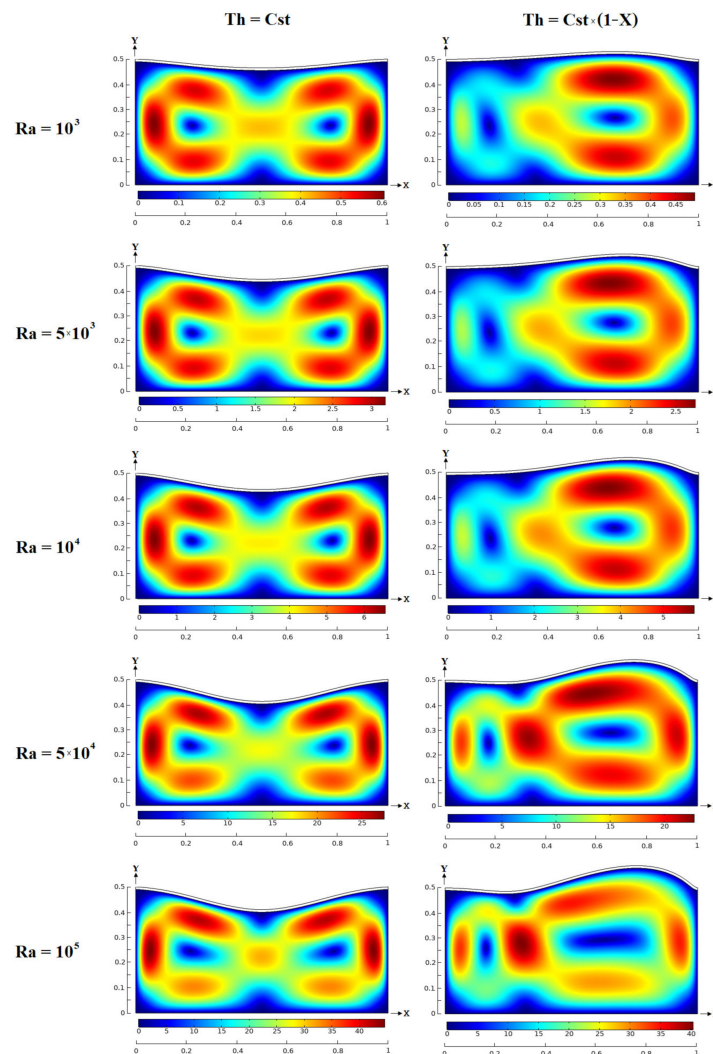


Figure 5. Combined effects of hot temperature distribution and Rayleigh number on nanofluid velocity magnitude distribution.

Figure 4 shows that, as the Rayleigh number increases from $Ra = 10^3$ to $Ra = 10^5$, heat transfer becomes dominated by convection instead of conduction. This is due to the enhancement of the buoyancy effect when the Rayleigh number increases. The nanofluid temperature becomes more homogenous, especially in the central zone, away from the hot and cold walls. This is expected, since the temperature difference from the upper fluid region (close to the hot plate) and the lower region (far from the hot plate) is rapidly and considerably reduced, since there is no direct and constant cooling effect imposed by the cold wall temperature in the central region. This cooling direct effect considerably retards the nanofluid's temperature homogeneity in its vicinity, despite strong heat transfer with hot nanofluid zones due to high temperature differences. Thus, the nanofluid close to the cold wall remains relatively cold compared to the quite homogenous nanofluid temperature in the central zone of the enclosure.

The nanofluid temperature contours are symmetric and dominated by the hot wall in the case where the imposed hot temperature distribution is uniform along the hot wall, whereas they are asymmetric and dominated by the cold walls in the case where the imposed hot temperature distribution is right-triangular. This is due to the fact that the right-triangular imposed temperature represents a decreasing linear evolution from the left to the right side of the plate. The hot temperature effect is concentrated in the left side of the plate. The remaining region of the plate is considered to have a colder and colder

temperature while moving towards the right side of the plate. Thus, the hot temperature effect loses, naturally, its symmetry on nanofluid temperature contours.

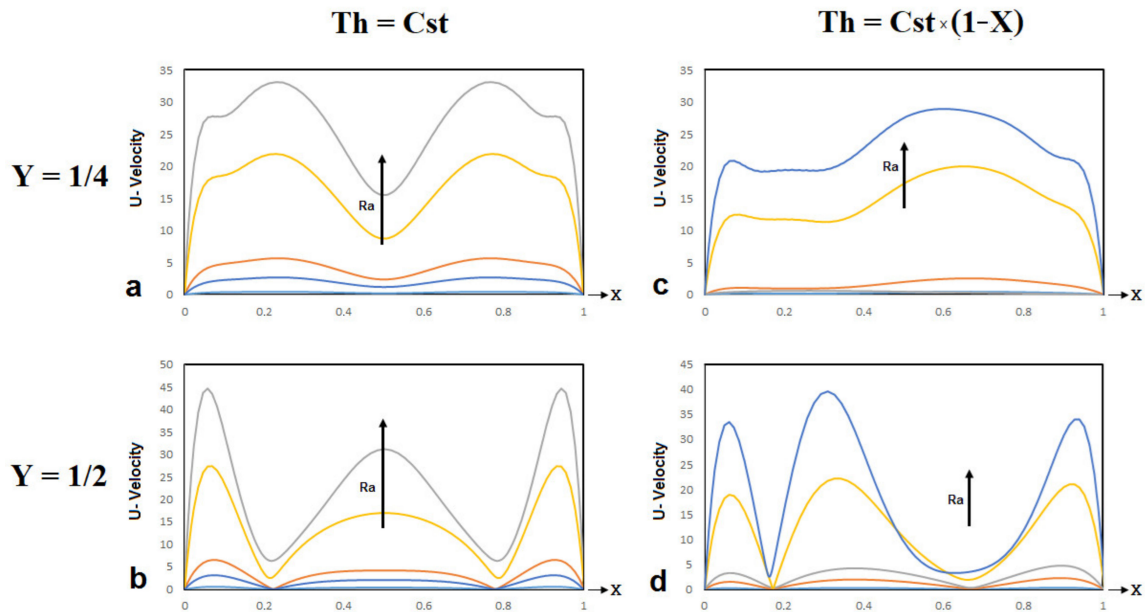


Figure 6. Combined effects of hot temperature distribution and Rayleigh number on nanofluid velocity magnitude evolutions along x -axis: (a) Imposed hot temperature $Th = Cst$ and Level $Y = 1/4$; (b) Imposed hot temperature $Th = Cst$ and Level $Y = 1/2$; (c) Imposed hot temperature $Th = Cst \times (1 - X)$ and Level $Y = 1/4$; (d) Imposed hot temperature $Th = Cst \times (1 - X)$ and Level $Y = 1/2$.

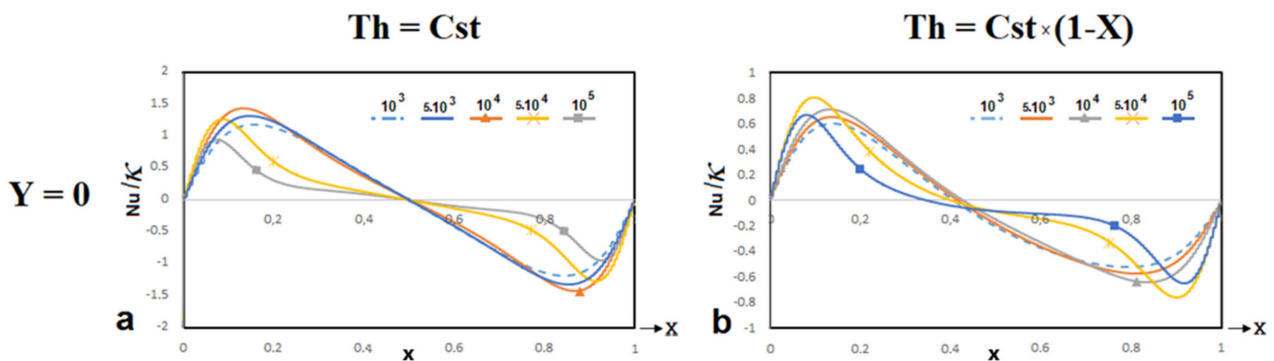


Figure 7. Combined effects of hot temperature distribution and Rayleigh number on Nusselt number evolutions along x -axis: (a) Imposed hot temperature $Th = Cst$ and Level $Y = 0$; (b): Imposed hot temperature $Th = Cst \times (1 - X)$ and Level $Y = 1/2$.

Figure 5 shows that, as the Rayleigh number increases from $Ra = 10^3$ to $Ra = 10^5$, the nanofluid velocity magnitude is enhanced. This is due to the fact that an increase in the Rayleigh number reflects a greater buoyancy effect, which enhances nanofluid velocity. For a uniform imposed hot temperature, the minimum velocity magnitude is reached in the central zones of the left and the right cavities as well as near the wall enclosure, whereas the maximum velocity magnitude is reached symmetrically around these two central zones. This is expected, since the zones of minimum and maximum velocity are characterized, respectively, by strong buoyancy (due to high density differences) and weak buoyancy (due to low density differences) across these zones. The noticed symmetry is due, naturally, to the uniform distribution of the imposed hot temperature along the hot plate. For a right-triangular imposed hot temperature, the same maximum magnitude velocity phenomenon is encountered, except that it globally migrates towards the right cavity. This non-symmetry is due to the fact that the decreasing linear evolution (from

left to right) of the imposed hot temperature on the plate induces the migration of a high density difference zone towards the right cavity of the enclosure.

Figure 6 shows that, as the Rayleigh number increases, the extrema reached by the velocity magnitude evolutions along the enclosure's x -direction become higher. This is due to the enhancement of buoyancy for higher Rayleigh numbers. At higher Rayleigh numbers, the extrema are more pronounced as they are closer to the hot wall. This is expected based on the examination of the velocity magnitude distribution depicted by Figure 5. For a uniform imposed hot temperature, the velocity magnitude evolutions are symmetric, whereas they lose symmetry for a right-triangular imposed hot temperature, especially for $Ra = 5 \times 10^4$ and $Ra = 10^5$. This non-symmetry is more pronounced at higher Rayleigh numbers. This is due to the fact that the effect of the decreasing linear evolution of the imposed hot temperature is more visible when buoyancy is more important (high Rayleigh number).

Figure 7 shows that, as the Rayleigh number increases from $Ra = 10^3$ to $Ra = 10^5$, the maximum value reached by the nanofluid Nusselt number approaches closer and closer to the cold walls. For a uniform imposed hot temperature, the Nusselt number reaches higher values than those attained for a right-triangular imposed hot temperature. This is due to the fact that the zones where heat transfer is carried out by convection instead of conduction are near cold walls, since the buoyancy is more pronounced in these zones. The symmetry of Nusselt number evolutions is globally not affected by the imposed hot temperature distribution.

5.3. Combined Effect of Hot Temperature Distribution and Air Pressure

The combined effect of hot temperature distributions and air pressure on nanofluid temperature contours (Figure 8) was numerically investigated.

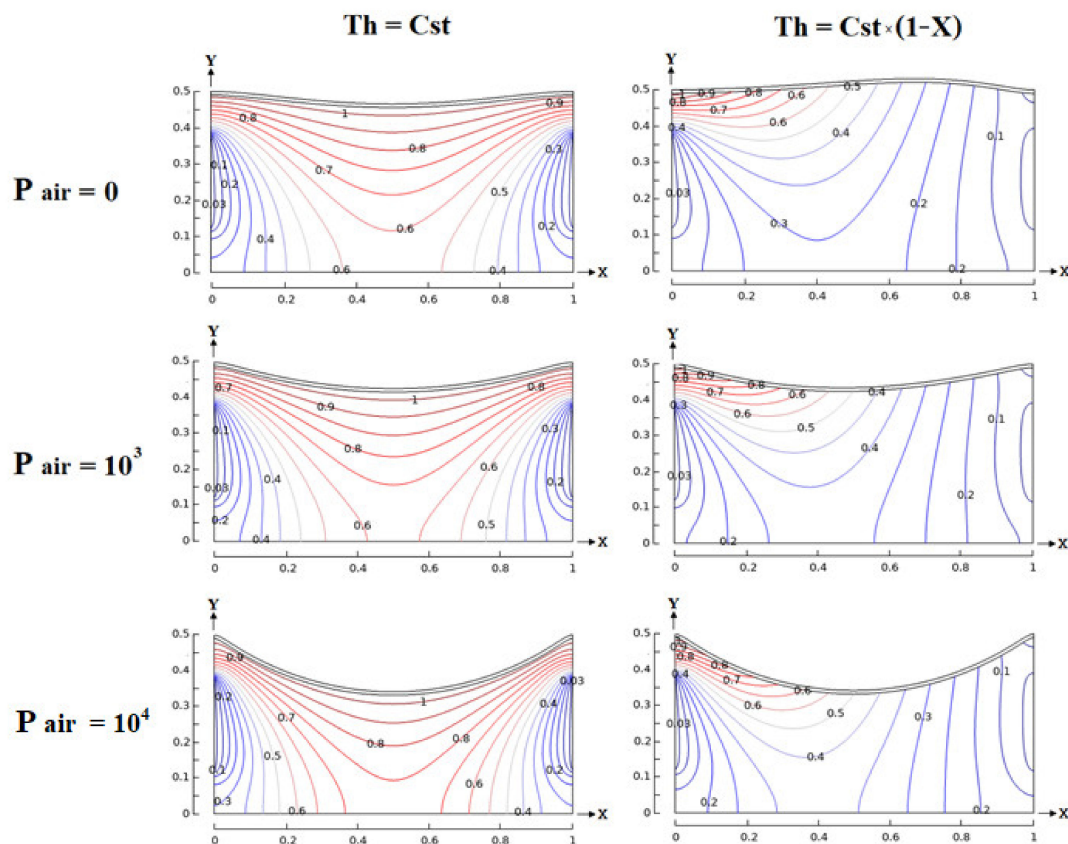


Figure 8. Combined effects of hot temperature distribution and air pressure on nanofluid temperature contour.

Figure 8 shows that, as the air pressure increases from $P_{\text{air}} = 0$ Pa to $P_{\text{air}} = 10^4$ Pa, heat transfer becomes dominated by convection instead of conduction, and the nanofluid temperature is homogenized, particularly in the central zone away from the hot and cold walls. The temperature contours are symmetric and strongly affected by the hot wall when the imposed hot temperature distribution is uniform. The temperature contours become asymmetric and strongly affected by the cold walls when the imposed hot temperature distribution is right-triangular. The air pressure does not affect the temperature contour symmetry.

6. Conclusions

The current numerical investigation shows that, as the Rayleigh number increases from $Ra = 10^3$ to $Ra = 10^5$, heat transfer within the nanofluid becomes dominated by convection instead of conduction, mainly in the central zone of the enclosure, far from the hot and cold imposed temperature on the walls. When the imposed hot temperature on the plate is uniformly distributed, the symmetry of the nanofluid temperature contours is more noticeable and particularly influenced by the hot wall. This temperature contour symmetry is deteriorated when the imposed hot temperature distribution is linearly decreased from the left to the right of the plate. Moreover, increases in the Rayleigh number amplify the global velocity magnitude of the nanofluid. When the imposed hot temperature on the plate is uniformly distributed, the velocity magnitude distribution is left and right-symmetric within the enclosure. This symmetry is deteriorated when the imposed hot temperature distribution is linearly decreased from the left to the right of the plate. Moreover, it is worth noting that, as the Rayleigh number increases, the velocity magnitude extrema reached along the x -direction of the enclosure are amplified and more pronounced close to the hot wall. For Rayleigh numbers $Ra = 5 \times 10^4$ and higher, the symmetry of the velocity magnitude extrema is deteriorated in the case where the imposed hot temperature distribution is linearly decreased from the left to the right of the plate. The maximum nanofluid Nusselt number (describing the ratio of heat transfer by convection and heat transfer by conduction) is pushed towards the cold walls as the Rayleigh number increases. Furthermore, the Nusselt number is enhanced in the case where the imposed hot temperature on the plate is uniformly distributed. As the air pressure in the upper enclosure increases from $P_{\text{air}} = 0$ Pascal to $P_{\text{air}} = 10^4$ Pascal, heat transfer in the nanofluid becomes dominated by convection, mainly in the central zone of the nanofluid enclosure. Temperature contours are highly influenced by the hot plate in the case where the imposed hot temperature is uniformly distributed on the plate. Increases in air pressure do not affect the symmetry of temperature contours in the nanofluid enclosure. The current study does not consider the effect of the magnetic field's magnitude and inclination, as well as the elastic modulus of the plate, on the thermal and flow behavior of the nanofluid. This will be the scope of the next research investigation as a continuation of the current one.

Author Contributions: Conceptualization, R.N. and F.A.; methodology, R.N.; software, F.A.; validation, C.A., R.N. and F.A.; formal analysis, F.N.; investigation, R.N.; resources, F.N.; data curation, F.A.; writing—original draft preparation, R.N.; writing—review and editing, F.A.; visualization, C.A.; supervision, F.N.; project administration, F.A.; funding acquisition, F.N. All authors have read and agreed to the published version of the manuscript.

Funding: This research was funded by the Deanship of Scientific Research at Bisha University.

Institutional Review Board Statement: Not applicable.

Informed Consent Statement: Not applicable.

Data Availability Statement: Not applicable.

Acknowledgments: The authors would like to thank the Deanship of Scientific Research at Bisha University for supporting this work.

Conflicts of Interest: The authors declare no conflict of interest.

Nomenclature

a	Local acceleration
C_p	Specific heat capacity
D	Average particle size
D	Displacement vector
f_b	Body forces
h	Convective heat transfer coefficient
k	Effective thermal conductivity
n	Normal direction
Nu	Nusselt number
P	Pressure
Ra	Rayleigh number
T	Temperature
\vec{u}	Nanofluid velocity vector
u	x-component of the velocity
u_g	Moving coordinate velocity
v	y-component of the velocity
X	Dimensionless x -direction
Y	Dimensionless y -direction
Greek symbol	
α	Thermal diffusivity
β	Coefficient of thermal expansion
ϕ	Solid volume fraction
κ	Thermal conductivity ratio = $-k_f/k_{nf}$
μ	Effective viscosity
ρ	Density
$\vec{\sigma}$	Stress tensor
Subscript	
abs	Absorber
amb	Ambient
air	Air
c	Cold
cv	Convection
f	Fluid
$glass$	Glass
h	Hot
nf	Nanofluid
p	Nanoparticle
s	Solid
st	Static

References

- Hatami, M.; Jing, D. *Nanofluids: Mathematical, Numerical, and Experimental Analysis*; Academic Press: Cambridge, MA, USA, 2020; ISBN 978-0-08-102933-6. [[CrossRef](#)]
- Mahbubul, I.M. *Preparation, Characterization, Properties and Application of Nanofluid*; William Andrew: Norwich, NY, USA, 2019; ISBN 978-0-12-813245-6. [[CrossRef](#)]
- Das, S.K.; Choi, S.U.; Yu, W.; Pradeep, T. *Nanofluids: Science and Technology*; Wiley: Hoboken, NJ, USA, 2007; ISBN 978-0-470-07473-2.
- Murshed, S.; Nieto, D.C. *Nanofluids: Synthesis, Properties and Applications*; Nova Science Pub Inc.: Hauppauge, NY, USA, 2014; ISBN 978-1633216778.
- Sheikholeslami, M.; Ganji, D.D. *Applications of Nanofluid for Heat Transfer Enhancement*; William Andrew: Norwich, NY, USA, 2017; ISBN 978-0-08-102172-9.
- Xuan, Y.; Li, Q. Heat transfer enhancement of nanofluids. *Int. J. Heat Fluid Flow* **2000**, *21*, 58–64. [[CrossRef](#)]
- Bianco, V.; Manca, O.; Vafai, S.N.K. *Heat Transfer Enhancement with Nanofluids*; CRC Press: Boca Raton, FL, USA, 2017; ISBN 9781138749481.
- Ali, H. *Advances in Nanofluid Heat Transfer*; Elsevier: Amsterdam, The Netherlands, 2022; ISBN 9780323886567.
- Das, S.K.; Choi, S.U.S.; Patel, H.E. Heat Transfer in Nanofluids—A Review. *Heat Transf. Eng.* **2006**, *27*, 3–19. [[CrossRef](#)]
- Kamyar, A.; Saidur, R.; Hasanuzzaman, M. Application of Computational Fluid Dynamics (CFD) for nanofluids. *Int. J. Heat Mass Transf.* **2012**, *55*, 4104–4115. [[CrossRef](#)]

11. Karimi, Y.; Nazar, A.R.S.; Motevasel, M. CFD simulation of nanofluid heat transfer considering the aggregation of nanoparticles in population balance model. *J. Therm. Anal. Calorim.* **2021**, *143*, 671–684. [[CrossRef](#)]
12. Chummar, A.; Harish, R. CFD simulation of laminar free convection flows of nanofluids in a cubical enclosure. *Mater. Today Proc.* **2022**, *51*, 1473–1481. [[CrossRef](#)]
13. Behroyan, I.; Ganesan, P.; He, S.; Sivasankaran, S. CFD models comparative study on nanofluids subcooled flow boiling in a vertical pipe. *Numer. Heat Transf. Part A Appl.* **2018**, *73*, 55–74. [[CrossRef](#)]
14. Bognár, G.; Klazly, M.; Hriczó, K. Nanofluid Flow Past a Stretching Plate. *Processes* **2020**, *8*, 827. [[CrossRef](#)]
15. Pozorski, J.; Waclawczyk, M. Mixing in Turbulent Flows: An Overview of Physics and Modelling. *Processes* **2020**, *8*, 1379. [[CrossRef](#)]
16. Selimefendigil, F.; Öztop, H.F. Magnetohydrodynamics with Nanofluids for Heat Transfer Applications. In *Advances in New Heat Transfer Fluids*; CRC Press: Boca Raton, FL, USA, 2017; ISBN 9781315368184.
17. Cao, Y.; Ayed, H.; Jarad, F.; Togun, H.; Alias, H.; Issakhov, A.; Dahari, M.; Wae-hayee, M.; El Ouni, M.H. MHD natural convection nanofluid flow in a heat exchanger: Effects of Brownian motion and thermophoresis for nanoparticles distribution. *Case Stud. Therm. Eng.* **2021**, *28*, 101394. [[CrossRef](#)]
18. Hamarshah, A.S.; Alwawi, F.A.; Alkassabeh, H.T.; Rashad, A.M.; Idris, R. Heat Transfer Improvement in MHD Natural Convection Flow of Graphite Oxide/Carbon Nanotubes-Methanol Based Casson Nanofluids Past a Horizontal Circular Cylinder. *Processes* **2020**, *8*, 1444. [[CrossRef](#)]
19. Faraz, F.; Haider, S.; Imran, S.M. Study of magneto-hydrodynamics (MHD) impacts on an axisymmetric Casson nanofluid flow and heat transfer over unsteady radially stretching sheet. *SN Appl. Sci.* **2020**, *2*, 14. [[CrossRef](#)]
20. Moraveji, M.K.; Ardehali, R.M. CFD modeling (comparing single and two-phase approaches) on thermal performance of Al₂O₃/water nanofluid in mini-channel heat sink. *Int. Commun. Heat Mass Transf.* **2013**, *44*, 157–164. [[CrossRef](#)]
21. Moraveji, M.K.; Esmaeili, E. Comparison between single-phase and two-phases CFD modeling of laminar forced convection flow of nanofluids in a circular tube under constant heat flux. *Int. Commun. Heat Mass Transf.* **2012**, *39*, 1297–1302. [[CrossRef](#)]
22. Akbari, M.; Galanis, N.; Behzadmehr, A. Comparative analysis of single and two-phase models for CFD studies of nanofluid heat transfer. *Int. J. Therm. Sci.* **2011**, *50*, 1343–1354. [[CrossRef](#)]
23. Ahmad, F.; Abdal, S.; Ayed, H.; Hussain, S.; Salim, S.; Almatroud, A.O. The improved thermal efficiency of Maxwell hybrid nanofluid comprising of graphene oxide plus silver/kerosene oil over stretching sheet. *Case Stud. Therm. Eng.* **2021**, *27*, 101257. [[CrossRef](#)]
24. Ahmed, K.; Akbar, T.; Muhammad, T.; Alghamdi, M. Heat transfer characteristics of MHD flow of Williamson nanofluid over an exponential permeable stretching curved surface with variable thermal conductivity. *Case Stud. Therm. Eng.* **2021**, *28*, 101544. [[CrossRef](#)]
25. Waqas, H.; Naqvi, S.M.R.S.; Alqarni, M.S.; Muhammad, T. Thermal transport in magnetized flow of hybrid nanofluids over a vertical stretching cylinder. *Case Stud. Therm. Eng.* **2021**, *27*, 101219. [[CrossRef](#)]
26. Awati, V.B.; Kumar, M.N.; Wakif, A. Haar wavelet scrutinization of heat and mass transfer features during the convective boundary layer flow of a nanofluid moving over a nonlinearly stretching sheet. *Partial Differ. Equ. Appl. Math.* **2021**, *4*, 100192. [[CrossRef](#)]
27. Hammachukiattikul, P.; Govindaraju, M.; Sohail, M.; Vadivel, R.; Gunasekaran, N.; Askar, S. Analytical Study on Sodium Alginate Based Hybrid Nanofluid Flow through a Shrinking/Stretching Sheet with Radiation, Heat Source and Inclined Lorentz Force Effects. *Fractal Fract.* **2022**, *6*, 68. [[CrossRef](#)]
28. Sohut, M.N.F.H.; Soid, S.K.; Abu Bakar, S.; Ishak, A. Unsteady Three-Dimensional Flow in a Rotating Hybrid Nanofluid over a Stretching Sheet. *Mathematics* **2022**, *10*, 348. [[CrossRef](#)]
29. Yacob, N.A.; Dzulkipli, N.F.; Salleh, S.N.A.; Ishak, A.; Pop, I. Rotating Flow in a Nanofluid with CNT Nanoparticles over a Stretching/Shrinking Surface. *Mathematics* **2022**, *10*, 7. [[CrossRef](#)]
30. Ramzan, M.; Gul, H.; Malik, M.Y.; Hassan, A.S.G. Entropy Minimization Analysis of a Partially Ionized Casson Nanofluid Flow over a Bidirectional Stretching Sheet with Surface Catalyzed Reaction. *Arab. J. Sci. Eng.* **2022**, 1–13. [[CrossRef](#)]
31. Bhatti, M.M.; Shahid, A.; Abbas, T.; Alamri, S.Z.; Ellahi, R. Study of Activation Energy on the Movement of Gyrotactic Microorganism in a Magnetized Nanofluids Past a Porous Plate. *Processes* **2020**, *8*, 328. [[CrossRef](#)]
32. Henein, S.M.; Abdel-Rehim, A.A. The performance response of a heat pipe evacuated tube solar collector using MgO/MWCNT hybrid nanofluid as a working fluid. *Case Stud. Therm. Eng.* **2022**, *33*, 101957. [[CrossRef](#)]
33. Soni, P.; Verma, F.K.; Ranjan, R.; Gaba, V.K. Performance analysis of shell and helical tube heat exchanger using CuO/water and Al₂O₃/water nanofluids. *World J. Eng.* **2022**, in press. [[CrossRef](#)]
34. Imran, W.M.; Yasmin, S.; Waqas, H.; Khan, S.A.; Muhammad, T.; Alshammari, N.; Hamadneh, N.N.; Khan, I. Computational Analysis of Nanoparticle Shapes on Hybrid Nanofluid Flow Due to Flat Horizontal Plate via Solar Collector. *Nanomaterials* **2022**, *12*, 663. [[CrossRef](#)]
35. Akshay, C.; Soni, P.; Dhiman, S.K.; Bhowmick, S.; Gaba, V.K. Thermal modelling of single and double slope passive solar stills for different climatic zones in India. *Int. J. Ambient Energy* **2021**. [[CrossRef](#)]
36. Mustafa, I.; Javed, T.; Ghaffari, A. Heat transfer in MHD stagnation point flow of a ferrofluid over a stretchable rotating disk. *J. Mol. Liq.* **2016**, *219*, 526–532. [[CrossRef](#)]

37. Hayat, T.; Qayyum, S.; Imtiaz, M.; Alzahrani, F.A. Partial slip effect in flow of magnetite-Fe₃O₄ nanoparticles between rotating stretchable disks. *J. Magn. Magn. Mater.* **2016**, *413*, 39–48. [[CrossRef](#)]
38. Mustafa, M.; Mushtaq, A.; Hayat, T.; Alsaedi, A. Rotating Flow of Magnetite-Water Nanofluid over a Stretching Surface Inspired by Non-Linear Thermal Radiation. *PLoS ONE* **2016**, *11*, e0149304. [[CrossRef](#)]
39. Selimefendigil, F.; Öztop, H.F. Mixed convection in a two-sided elastic walled and SiO₂ nanofluid filled cavity with internal heat generation: Effects of inner rotating cylinder and nanoparticle's shape. *J. Mol. Liq.* **2015**, *212*, 509–516. [[CrossRef](#)]
40. Selimefendigil, F.; Öztop, H.F.; Abu-Hamdeh, N. Mixed convection due to rotating cylinder in an internally heated and flexible walled cavity filled with SiO₂-water nanofluids: Effect of nanoparticle shape. *Int. Commun. Heat Mass Transf.* **2016**, *71*, 9–19. [[CrossRef](#)]
41. Selimefendigil, F.; Oztop, H.F.; Chamkha, A.J. MHD mixed convection in a nanofluid filled vertical lid-driven cavity having a flexible fin attached to its upper wall. *J. Therm. Anal. Calorim.* **2019**, *135*, 325–340. [[CrossRef](#)]
42. Selimefendigil, F.; Oztop, H.F. Fluid-solid interaction of elastic-step type corrugation effects on the mixed convection of nanofluid in a vented cavity with magnetic field. *Int. J. Mech. Sci.* **2019**, *152*, 185–197. [[CrossRef](#)]